Microscopic study of compound-nucleus formation in cold-fusion reactions

Xiang-Xiang Sun (孙向向) and Lu Guo (郭璐)*

School of Nuclear Science and Technology, University of Chinese Academy of Sciences, Beijing 100049, China
and CAS Key Laboratory of Theoretical Physics, Institute of Theoretical Physics, Chinese Academy of Sciences, Beijing 100190, China

(Received 6 April 2022; accepted 3 May 2022; published 23 May 2022)

The understanding of fusion probability is of particular importance to reveal the mechanism of producing superheavy elements. We present a microscopic study of compound-nucleus formation by combining time-dependent density-functional theory, the coupled-channels approach, and dynamical diffusion models. The fusion probability and compound-nucleus formation cross sections for cold-fusion reactions ^{48}Ca + ^{208}Pb, ^{50}Ti + ^{208}Pb, and ^{54}Cr + ^{208}Pb are investigated and it is found that the deduced capture barriers and capture cross sections for these reactions are consistent with experimental data. Above the capture barrier, our calculations reproduce the measured fusion probability reasonably well. Our studies demonstrate that the restrictions from the microscopic dynamics theory improve the predictive power of the coupled-channels and diffusion calculations.

DOI: 10.1103/PhysRevC.105.054610

I. INTRODUCTION

The study of superheavy elements (SHEs) is one of the most important topics in nuclear physics nowadays [1–4]. The cross section of fusion-evaporation reactions for producing superheavy nuclei (SHN) is extremely small, on the order of 10^{-36} cm^2, and strongly dependent on the combination of two colliding nuclei and the incident energy. Up to now, SHEs up to $Z = 118$ have been synthesized by employing two types of fusion reactions in the laboratory: The cold-fusion reactions with ^{208}Pb and ^{209}Bi as targets [1,5] and hot-fusion reactions between ^{48}Ca and actinide nuclei [6,7]. The former lead to the discoveries of new elements up to $Z = 113$ and the latter for SHN with $113 \leqslant Z \leqslant 118$ so far. Lots of efforts have been made to produce SHN with $Z = 119$ and $Z = 120$ [8–12], but there is no evidence for the synthesis of new elements.

It is significant to understand the reaction dynamics to choose the appropriate combination of projectile and target nuclei to produce new SHN. Conceptually, the fusion-evaporation reaction can be divided into three steps, namely, the capture process, the fusion process, and the deexcitation of the excited compound nucleus (CN) against fission and light particle emission. The capture process is generally treated as a one-dimensional quantum tunneling under a given ion-ion potential with consideration of the couplings to the excitations of projectile and target nuclei [13,14] and the results from semi-empirical systematic [15–17] and coupled-channels calculations [13] are well consistent with measurements [18–21]. For the deexcitation process, the survival probability of CN is well studied with the statistical models [16,22] and the dependence on reaction parameters is also well understood, although it is strongly influenced by the fission-barrier height. Therefore, most theoretical approaches used to estimate the evaporation-residue cross sections have similar conclusions on these two steps [15,16,23–33].

However, the fusion process is still not well understood up to now. The calculated fusion probabilities with empirical formulas, master equations, or diffusion models differ by several orders of magnitude [15,22,25,27,33–37]. Even more, the dependence of the fusion probability on the reaction entrance channel is not well established [35,36,38]. Experimentally, the fusion probability can be extracted from the measurement of fusion-evaporation residue cross sections [39,40], comparing the width of fragment mass distribution with the width expected in the case of pure fusion-fission [21,41,42] or the analysis of the fragment angular distribution [43–45]. In recent years, many efforts have been made to measure the fusion probability and lots of progress has been achieved [46]. Very recently, experimentalists have extracted the fusion probabilities for both cold-fusion and hot-fusion reactions [21,35,45]. These measurements provide new constraints to theoretical investigations for the synthesis of SHN.

It has been shown that the macroscopic models can reproduce the cross-section data, but a lot of adjustable parameters are involved. In addition, the lack of dynamical effect challenges its predictive power for reactions without available experimental data. Modern dynamical microscopic approaches can provide insight into the low-energy heavy-ion collisions [47–50]. The time-dependent Hartree-Fock (TDHF) approach has been successfully applied to study many aspects of low-energy heavy-ion collisions (see Refs. [51–55] and references therein). Based on a mass of TDHF simulations, the fusion probability has been estimated by using the sharp-cutoff approximation for ^{48}Ca + ^{239,244}Pu at several selected incident energies [56]. However, this method is restrictive for a systematic study on fusion probabilities due to its computational cost. It has been shown that the TDHF simulations can provide the main ingredients of coupled-channels calculations for capture cross sections [57,58] and diffusion

*luguo@ucas.ac.cn

 ©2022 American Physical Society

processes [59]. Note that the TDHF approach is not suitable for the whole process of fusion-evaporation reactions. The purpose of the present work is to combine TDHF with both the coupled-channels and dynamic diffusion approaches, aiming at the systematic study of fusion probability. In this approach, one can eliminate the uncertainties of adjustable parameters for calculating capture and fusion cross sections under the restriction from microscopic TDHF theory, while the influences of the structures of reactants and dynamical effects can be taken into account. In this work, we use this method to study the systematics of the fusion probability of cold-fusion reactions.

This article is organized as follows: In Sec. II, we show the main theoretical formulation to calculate capture cross sections and fusion probabilities. Section III presents the calculational details and the discussion of results. A summary and perspective is provided in Sec. IV.

II. THEORETICAL FRAMEWORK

In the TDHF theory, the Hamiltonian $\hat{H}$ is a functional of densities and the dynamic process is described by the evolution of the one-body density $\hat{\rho}$, which is obtained by solving the TDHF equation

$$i\hbar\frac{\partial}{\partial t}\hat{\rho} = [\hat{H}[\hat{\rho}], \hat{\rho}]. \tag{1}$$

Since the TDHF theory describes the collective motion in a semiclassical way, the quantum tunneling of the many-body wave function is not included. Therefore, when studying capture cross sections by using the TDHF theory, a commonly applied and very effective strategy is using the ion-ion potential obtained from frozen HF [60], density constrained (DC) TDHF [47,49,57,58,61–66], DC frozen HF [67], dissipative-dynamics TDHF [50], the Thomas-Fermi approximation [68], and the Woods-Saxon (WS) potential with the fitted parameters [57] as the input of the coupled-channels code CCFULL [69] to calculate the penetration probability. In our approach, for a given colliding system, we perform TDHF calculations to determine the capture barrier, which is the minimum incident energy for which the projectile can be captured by the target in a TDHF simulation. The calculated densities in their ground states and the obtained capture barriers are then used to fix the parameters of the WS potential [70]:

$$V(R) = -\frac{V_0}{1+\exp\left(\frac{R-r_{0\mathrm{P}}A_{\mathrm{P}}^{1/3}-r_{0\mathrm{T}}A_{\mathrm{T}}^{1/3}}{a}\right)}, \tag{2}$$

with the depth V_0, the diffuseness parameter a, radius parameter for target (projectile) $r_{0\mathrm{T}}$ ($r_{0\mathrm{P}}$), and the mass number A_{T} (A_{P}) of the target (projectile). In this work, the diffuseness parameter is determined by

$$a = \frac{1}{1.17\left[1+0.53\left(A_{\mathrm{P}}^{-1/3}+A_{\mathrm{T}}^{-1/3}\right)\right]}\ \mathrm{fm}, \tag{3}$$

taken from Ref. [17], and the determination of V_0, $r_{0\mathrm{T}}$, and $r_{0\mathrm{P}}$ will be introduced later. Considering the coupling to low-lying states of projectile and target nuclei, the capture cross sections are obtained by using the standard coupled-channels calculations [69] and read

$$\sigma_{\mathrm{cap}}(E_{\mathrm{c.m.}}) = \frac{\pi}{k^2}\sum_J (2J+1)T_J(E_{\mathrm{c.m.}}), \tag{4}$$

where $k = (2\mu E_{\mathrm{c.m.}}/\hbar^2)^{1/2}$ with μ being the reduced mass in the entrance channel. $T_J(E_{\mathrm{c.m.}})$, which is calculated by using the incoming wave boundary condition method [69], is the penetration probability for given incident energy $E_{\mathrm{c.m.}}$ and angular momentum J. It should be noted that one can also use the DC-TDHF method to extract the microscopic internuclear potentials, but which needs much computational cost [64] for the reactions to produce SHN and the obtained potential depends on the incident energy. For a systematic study of fusion cross sections of cold-fusion reactions, the computational cost of the DC-TDHF is too high.

For the second stage of the fusion-evaporation reactions, the contact configuration of touching nuclei can be transformed to CN configuration by overcoming the inner barrier. In this process, before the formation of CN, quasifission happens and the heavy nuclear system is split into two fragments. Therefore, the formation of CN is strongly hindered by quasifission, which is dependent on the structure of the reactants and has also been studied by using the TDHF approach [56,64,71–74]. In the fusion-by-diffusion (FbD) model [15,29,75,76], the formation of CN is idealized as a one-dimensional diffusion over a parabolic barrier, and the corresponding probability is totally determined by the distance between the surfaces of two colliding nuclei at the injection point. This quantity can be estimated from the TDHF evolution by choosing the moment when the collective kinetic energy is completely dissipated into the internal degrees of freedom in the overdamped regime for a given incident energy, see Ref. [59] for details. It should be mentioned that, in Ref. [59], only s-wave scattering is considered and the penetration possibilities is obtained for one or two selected incident energies in the above-barrier region. In our approach, the fusion probability $P_{\mathrm{CN}}(E_{\mathrm{c.m.}}, J)$ at each angular momentum and incident energy is obtained by using the formulas given in Ref. [29].

The CN formation cross section is

$$\sigma_{\mathrm{fus}}(E_{\mathrm{c.m.}}) = \frac{\pi}{k^2}\sum_J (2J+1)T_J(E_{\mathrm{c.m.}})P_{\mathrm{CN}}(E_{\mathrm{c.m.}}, J). \tag{5}$$

Thus, one can study the systematics of the fusion probability by comparing the effective fusion probabilities P_{fus} defined as $\sigma_{\mathrm{fus}}/\sigma_{\mathrm{cap}}$ with measured ones.

III. RESULTS AND DISCUSSIONS

In a recent experiment [21], the upper limits of fusion probabilities for cold-fusion reactions of ^{48}Ca, ^{50}Ti, and ^{54}Cr with ^{208}Pb have been extracted systematically. Therefore it is quite interesting to examine whether our approach is valid for these reactions. The time evolution of each reaction system is obtained by using the modified version of the SKY3D code [77], which was also used to perform calculations in Refs. [56,58,65,66,78–82]. Recently, the density functional SLy5 [83] has been adopted in many investigations [47,56,58,65,66,81,82,84] and is also used in the

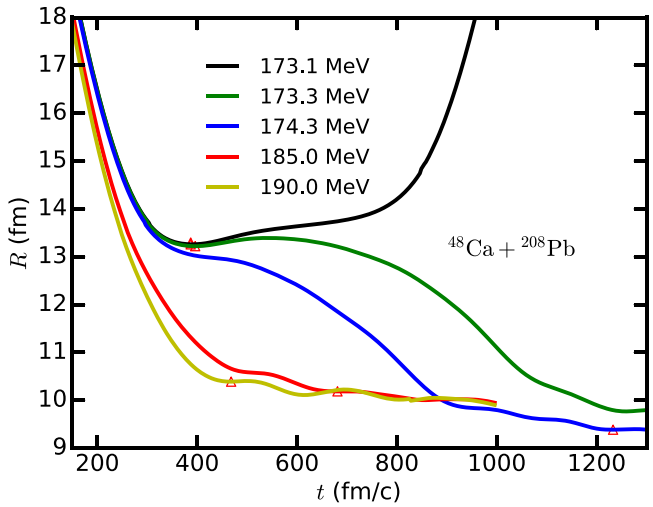

FIG. 1. Time evolution of the distance between the fragments in ^{48}Ca + ^{208}Pb central collisions. The open triangles represent the first moment with a zero canonical momentum.

present work. The ground states of ^{48}Ca, ^{50}Ti, ^{54}Cr, and ^{208}Pb are obtained by solving the static HF equation on a three-dimensional grid $28 \times 28 \times 28$ fm^3. To get a spherical ground state, the proton orbital $1f_{7/2}$ is fully filled with equal weight for ^{50}Ti and the proton orbital $1f_{7/2}$ and neutron orbital $2p_{3/2}$ are equally occupied for ^{54}Cr. We mention that ^{50}Ti is spherical due to the magic number $N = 28$ and ^{54}Cr has a prolate shape with quadrupole deformation parameter of 0.21 in static HF calculations. Thus this filling approximation is suitable for ^{50}Ti. Since in this work we disregard the orientation effects of the projectile, ^{54}Cr is also set to be spherical by the same strategy as used in Ref. [59]. The dynamic evolution for these three reactions are performed in a three-dimensional grid with the size of $60 \times 40 \times 40$ fm^3. The grid spacing in each direction is taken to be 1 fm and the time step is 0.2 fm/c. All the numerical conditions have been checked for achieving a good numerical accuracy for all the cases studied here.

To get the Coulomb barrier of each reaction system, we perform TDHF simulations of central collisions at different incident energies and around the barrier the step of the incident energy is taken to be 0.2 MeV. In Fig. 1, we show the time evolution of the separation distance between the fragments for ^{48}Ca + ^{208}Pb central collisions at several selected incident energies. This distance is determined by using the standard TDHF approach of finding left and right dividing planes and is the separation distance between the centers of the density in these two halves [47,77]. The time period 1300 fm/c is enough for these systems to come over the Coulomb barrier and to form the contact configuration, i.e., the projectile captured by the target. If one wants to get the fusion threshold energy or to judge quasifission, a much longer time TDHF simulation is needed [85]. It is clear that, when $E_{\rm c.m.} \geqslant$ 173.3 MeV, capture happens for ^{48}Ca + ^{208}Pb, in which the collective kinetic energy can be entirely converted into the internal excitation of the contacting system. Thus, the capture threshold energy $V_B^{\rm TDHF}$ for this reaction is 173.3 MeV. The first moment corresponding to a zero conjugate momentum of R at each reaction energy is represented by the open triangles in Fig. 1. We also perform similar calculations for ^{50}Ti + ^{208}Pb and ^{54}Cr + ^{208}Pb and the corresponding threshold energies are 191.4 and 209.4 MeV, respectively. The Coulomb barrier for these three reactions obtained from such TDHF calculations agree reasonably with those deduced from experimental capture cross sections by using a classical barrier-passing model for fissionlike cross sections, 173.4 ± 0.1, 192.6 ± 0.1, and 207.3 ± 0.3 MeV for ^{48}Ca, ^{50}Ti, and ^{54}Cr, respectively [21].

The radius parameters of the WS potential can be obtained from the ground-state density in static HF calculations. Taking ^{208}Pb as an example, the radius from the center of nucleus to the isosurface with half of the saturation density ($\rho_0 = 0.16$ fm^{-3}) is 6.672 fm. Then its radius parameter is $r_{0\rm T} = 6.67 \times 208^{-1/3}$ fm $= 1.126$ fm. Similarly, we have $r_{0\rm P} = 1.161$, 1.088, and 1.087 fm for ^{48}Ca, ^{50}Ti, and ^{54}Cr, respectively. The depth V_0 can be adjusted for reproducing the capture thresholds from TDHF calculations and they are 165.42, 251.998, and 225.07 MeV for reactions ^{48}Ca + ^{208}Pb, ^{50}Ti + ^{208}Pb, and ^{54}Cr + ^{208}Pb, respectively. It should be noted that the low-lying collective vibrations can also be estimated by the TDHF evolution with external fields. But for the systems in question, the low-lying spectra of these nuclei are well known. Therefore, we use the fitted WS potentials together with the experimental data of excitation energies and deformations taken to be the same as those provided in the supplement of Ref. [21] to calculate the capture cross section with the code CCFULL. Finally, the calculated capture cross sections $\sigma_{\rm cap}$ are shown in Fig. 2 and compared with experimental data and the results from the ECC model [17]. As we can see, for each reaction, our calculations are in agreement with the ECC results and reproduce the experimental data reasonably well.

In the recent work [21], the fissionlike cross sections are measured and also shown in Fig. 2. The corresponding capture cross sections are obtained by using the CCFULL calculations with the capture barriers from the classical barrier-passing model and experimental low-lying excitation information. It is shown that the capture cross sections are larger than the measured fissionlike cross sections and after scaling with suppression factors S, good agreements are achieved. This suppression might be due to the energy dissipation before reaching the Coulomb barrier [87,88]. Therefore, we also multiply capture cross sections in our calculations by the same suppression factors used in Ref. [21] and find scaled cross sections are more consistent with the measurements, shown in Fig. 2. In conclusion, by deducing the parameters involved in coupled-channels calculations from TDHF simulations, the capture cross sections can be well determined for both below- and above-barrier regions. These results demonstrate the effectiveness of our model.

For the calculations of $P_{\rm CN}$, the only input parameter in the FbD model is the injection parameter, which can be estimated by TDHF evolution [59] and is defined as

$$s_{\rm inj} = R_{\rm min} - R_{\rm P} - R_{\rm T}, \tag{6}$$

where $R_{\rm min}$ is the distance between two fragments at the injection point. In this work, we choose the first moment with a zero canonical momentum in the TDHF evolution as

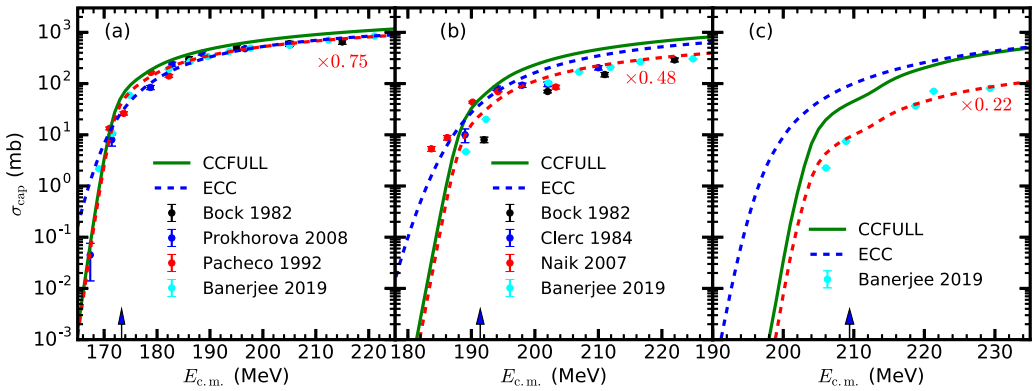

FIG. 2. Calculated capture cross sections for (a) ^{48}Ca + ^{208}Pb, (b) ^{50}Ti + ^{208}Pb, and (c) ^{54}Cr + ^{208}Pb. The calculated values with the ECC model [17] and the experimental data taken from Bock 1982 [86], Prokhorova 2008 [20], Pacheco 1992 [19], Clerc 1984 [18], Naik 2007 [35], and Banerjee 2019 [21] are shown for comparison. The capture thresholds are labeled by the up arrows for each reaction. The scaled cross sections are shown by the red dashed lines.

the injection point. In Fig. 1, we show the injection points labeled by open triangles for ^{48}Ca + ^{208}Pb for several selected incident energies. In this way, $R_{\rm min}$ is determined. The radii of colliding nuclei are estimated by using the empirical formula $R_i = r_{0i}A_i^{1/3}$ $(i = {\rm P, T})$ or taken to be the same as the root-mean-square matter radii in static HF calculation, which are 3.56, 3.59, 3.67, and 5.55 fm for ^{48}Ca, ^{50}Ti, ^{54}Cr, and ^{208}Pb, respectively. The calculated injection parameters corresponding to the empirical formula for the radius are labeled $s_{\rm inj}^{\rm I}$ and $s_{\rm inj}^{\rm II}$ for those with radii from static HF results. The values of $s_{\rm inj}$ from the empirical formulas used in the FbD model [29,89] are also shown for comparison. When $E_{\rm c.m.} - V_B^{\rm TDHF} > 4.59$ MeV, $s_{\rm inj}$ from the empirical formula given in Ref. [89] is taken to be zero. The shaded area in Fig. 3 means a derivation of ± 1 fm for the formula in Ref. [89].

In TDHF calculations, the contact configuration can only be reached in above-barrier reactions while the elastic scattering happens in below-barrier reactions. This leads to a sudden change of $s_{\rm inj}$. It is found that, for the below-barrier region, most values of $s_{\rm inj}^{\rm I}$ are located in the shaded area while $s_{\rm inj}^{\rm II}$ gives a much larger distance at the injection points compared with the empirical formula in FbD model. Above the barrier, the values of $s_{\rm inj}^{\rm I}$ are negative and most of them are well located at the shaded area, indicating that the overlap of the densities for two colliding nuclei is very large and results in a relatively large $P_{\rm CN}$. For $s_{\rm inj}^{\rm II}$, all of them are positive, indicating a small overlap of the densities and smaller $P_{\rm CN}$ compared with these for $s_{\rm inj}^{\rm I}$. Furthermore, $s_{\rm inj}$ extracted from TDHF calculations and the excess of incident energy also hold a linear relation in the below-barrier region, which is consistent with that fitted to experimental data shown in FbD model [15,29,30,32,89,90]. In the above-barrier region, most values of $s_{\rm inj}^{\rm I}$ and $s_{\rm inj}^{\rm II}$ are close to -0.6 and 1 fm, respectively, while the closet distance is usually taken to be zero in FdD calculations. In our method, $s_{\rm inj}$ is no longer an adjustable parameter in the FbD model, thus eliminating the uncertainties of the fusion cross section originating from $s_{\rm inj}$. Generally, the energy-dependence behavior of $s_{\rm inj}$ becomes weaker in above-barrier collisions compared with that in below-barrier region, i.e., the linear relation holding in the below-barrier region disappears in above-barrier collisions. This energy dependence behavior and the relevance with the entrance channel need to be explored further.

After obtaining the injection points by using formulas given in Ref. [29] with the nuclear data tables in Ref. [91] as inputs, we calculate the fusion probabilities $P_{\rm CN}(E_{\rm c.m.}, J)$ and fusion cross sections $\sigma_{\rm fus}$. To compare with the upper limits of measured fusion probabilities $P_{\rm sym}$ [21], we calculate the effective fusion probabilities $P_{\rm fus}$, defined as the ratio between fusion cross sections and capture cross sections in our model, which is independent of angular momenta. The upper panel

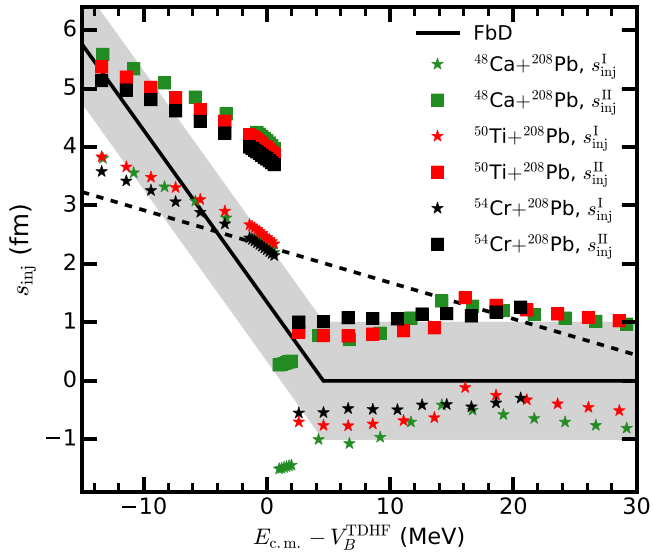

FIG. 3. The injection parameters $s_{\rm inj}^{\rm I}$ (stars) and $s_{\rm inj}^{\rm II}$ (squares) for reactions ^{48}Ca + ^{208}Pb (green), ^{50}Ti + ^{208}Pb (red), and ^{54}Cr + ^{208}Pb (black) obtained from TDHF simulations. $s_{\rm inj}$ from the empirical formulas given in Refs. [29,89] are labeled by black solid and dashed lines, respectively. The shaded area represents an error corridor of ± 1 fm for the formulas given in Ref. [89] and is drawn to guide the eye.

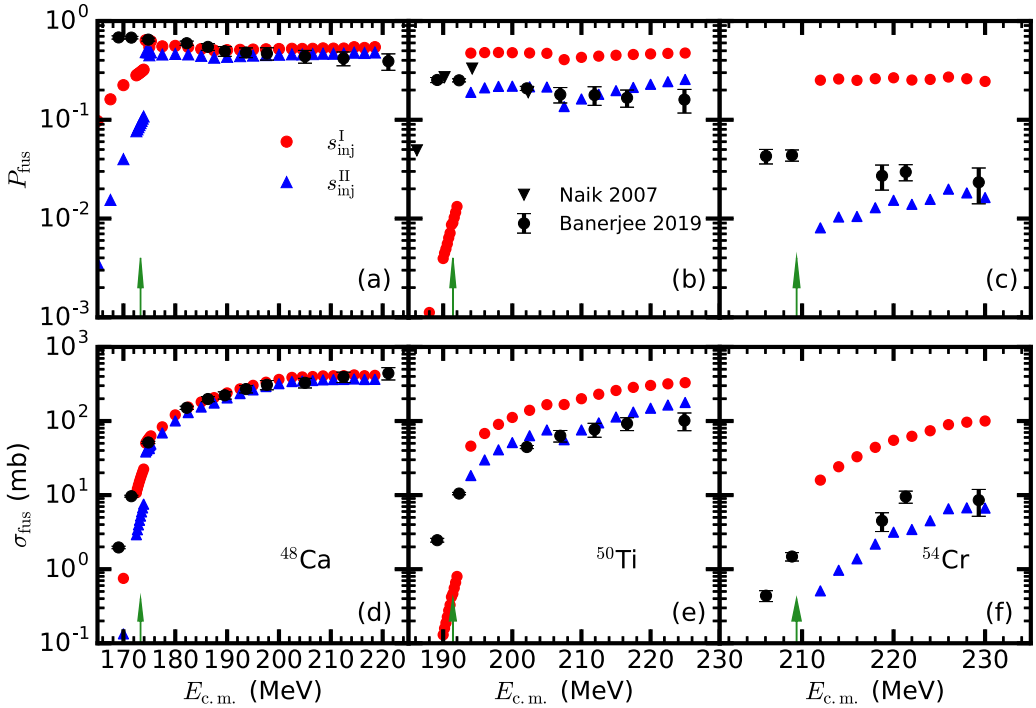

FIG. 4. The effective fusion probabilities (upper panel) and the fusion cross sections (bottom panel) for (a), (d) ^{48}Ca + ^{208}Pb, (b), (e) ^{50}Ti + ^{208}Pb, and (c), (f) ^{54}Cr + ^{208}Pb. Red circles (blue triangles) represent the calculated results with $s^{\rm I}_{\rm inj}$ ($s^{\rm II}_{\rm inj}$). The capture thresholds are labeled by the up arrows for each reaction. Experimental data taken from Banerjee 2019 [21] are shown by solid points with error bars. For ^{50}Ti + ^{208}Pb, the measurements from Naik 2007 [35] are presented by black triangles.

of Fig. 4 shows the comparison between calculated $P_{\rm fus}$ and $P_{\rm sym}$ taken from Ref. [21]. For ^{50}Ti + ^{208}Pb, the measurements given in Ref. [35] are presented by black triangles and shown in Fig. 4(b). The discontinuity of calculated $P_{\rm fus}$ around the barrier is due to the sudden change of $s_{\rm inj}$. Compared with experimental data in the below-barrier region, our calculated results are smaller than $P_{\rm sym}$ obviously. It is found that our calculations with $s^{\rm I}_{\rm inj}$ overestimate the experimental data while the results with $s^{\rm II}_{\rm inj}$ well reproduce the measurements in the above-barrier region. The differences of $P_{\rm fus}$ between the calculations with $s^{\rm I}_{\rm inj}$ and $s^{\rm II}_{\rm inj}$ become larger from ^{48}Ca to ^{54}Cr, because the height of the inner barrier is more sensitive to the injection parameter with the increase of the charge number of CN [15]. Our calculations demonstrate that a precise determination of $s_{\rm inj}$ is necessary for achieving a reasonable description of fusion probability and our method can well reproduce the data of above-barrier collisions.

By using the experimental data of fissionlike cross section $\sigma_{\rm fis}$ and the upper limit of fusion probability $P_{\rm sym}$ given in Ref. [21], the experimental fusion cross section can be estimated as $\sigma_{\rm fis}P_{\rm sym}/S$, where S is the suppression factor used in Ref. [21]. We compare our results of fusion cross section $\sigma_{\rm fus}$ [cf. Eq. (5)] with those deduced from measurements [21] in the bottom panel of Fig. 4, although they are not fully equivalent. For the region $E_{\rm c.m.} < V_B^{\rm TDHF} + 2$ MeV, the calculations with both $s^{\rm I}_{\rm inj}$ and $s^{\rm II}_{\rm inj}$ are smaller than the data by about an order of magnitude, while for the other region, a good agreement is achieved by the calculations with $s^{\rm II}_{\rm inj}$. Generally speaking, $P_{\rm fus}$ and $\sigma_{\rm fus}$ of below-barrier collisions are not well reproduced but for above-barrier collisions, our calculations with $s^{\rm II}_{\rm inj}$ are well consistent with the data. Among these three reaction systems, the differences between experimental data and our calculations with $s^{\rm II}_{\rm inj}$ are largest for ^{54}Cr + ^{208}Pb. This might be because the static deformation effects and dynamic pairing are not included in the present investigation. In addition, during the TDHF evolution, the dynamic changes of the shapes for the colliding nuclei influence the radii $R_{\rm T}$ and $R_{\rm P}$ at the injection points, leading to changes of injection parameters that affect fusion probabilities further. In this work, we use the fitted WS potentials that assumes frozen shapes, and its combination with the threshold energy deduced from TDHF might also be a source of discrepancy.

IV. SUMMARY AND PERSPECTIVE

We present a microscopic calculation of the fusion probability and the CN formation cross section by combining the TDHF with the coupled-channels approach and the FbD model. The capture cross section is obtained by performing coupled-channels calculations, in which the involved parameters of the WS potential are fixed by using the ground-states properties from the static HF calculations and capture thresholds determined from TDHF simulations. The fusion probability is given by using the FbD model with only one input parameter, the injection-point distance, which is estimated by the time evolution of two colliding nuclei with the TDHF approach. We apply our model to the cold-fusion reactions ^{48}Ca + ^{208}Pb, ^{50}Ti + ^{208}Pb, and ^{54}Cr + ^{208}Pb. The

dynamic evolution of the central collisions in both below- and above-barrier regions are obtained with the effective interaction SLy5. It is found that the capture thresholds from TDHF calculations are in line with those extracted from measurements and the capture cross sections can well reproduce the experimental data. By estimating the injection points with the TDHF approach, the fusion probabilities and resulted CN formation cross sections agree reasonably with experiments.

In the present work, the ground states of the target and projectile nuclei are all spherical or restricted to be spherical. For hot-fusion reactions, it is necessary to take static deformation into account since most actinide nuclei are deformed in their ground states and the orientation in the entrance channel also affects the TDHF dynamic evolution, the capture cross section, and the injection point. The orientation effects can be taken into account in both capture and fusion processes by rotating the initial wave function of reactants in TDHF simulation. This generalization is our next step. Additionally, it should be mentioned that the dynamic process of colliding nuclei is very complicated and the formation of CN from contact configuration undergoes complex evolution of shape degrees of freedom. This challenges the definition of the surfaces for two colliding nuclei. Finally, we hope that our microscopic approach can provide new and reliable supports for choosing the optimal combination of target and projectile nuclei for the synthesis of the SHEs with $Z = 119$ and $Z = 120$ in the future.

ACKNOWLEDGMENTS

We thank Liang Li, Yun Huang, Zhen-Ji Wu, Bing Wang, Bing-Nan Lu, and Shan-Gui Zhou for helpful discussions. This work has been supported by the Strategic Priority Research Program of Chinese Academy of Sciences (Grants No. XDB34010000 and No. XDPB15) and the National Natural Science Foundation of China (Grants No. 11975237, No. 11575189, and No. 11790325). The results described in this paper are obtained on the High-performance Computing Cluster of ITP-CAS and the ScGrid of the Supercomputing Center, Computer Network Information Center of Chinese Academy of Sciences.

[1] S. Hofmann and G. Münzenberg, The discovery of the heaviest elements, Rev. Mod. Phys. **72**, 733 (2000).

[2] J. H. Hamilton, S. Hofmann, and Y. T. Oganessian, Search for superheavy nuclei, Annu. Rev. Nucl. Part. Sci. **63**, 383 (2013).

[3] Y. T. Oganessian and V. K. Utyonkov, Super-heavy element research, Rep. Prog. Phys. **78**, 036301 (2015).

[4] S. A. Giuliani, Z. Matheson, W. Nazarewicz, E. Olsen, P.-G. Reinhard, J. Sadhukhan, B. Schuetrumpf, N. Schunck, and P. Schwerdtfeger, Colloquium: Superheavy elements: Oganesson and beyond, Rev. Mod. Phys. **91**, 011001 (2019).

[5] K. Morita, K. Morimoto, D. Kaji, T. Akiyama, S.-i. Goto, H. Haba, E. Ideguchi, R. Kanungo, K. Katori, H. Koura, H. Kudo, T. Ohnishi, A. Ozawa, T. Suda, K. Sueki, H.-S. Xu, T. Yamaguchi, A. Yoneda, A. Yoshida, and Y.-L. Zhao, Experiment on the synthesis of element 113 in the reaction ^{209}Bi(^{70}Zn, n)^{278}113, J. Phys. Soc. Jpn. **73**, 2593 (2004).

[6] Y. Oganessian, Heaviest nuclei from ^{48}Ca-induced reactions, J. Phys. G **34**, R165 (2007).

[7] Y. T. Oganessian, F. S. Abdullin, P. D. Bailey, D. E. Benker, M. E. Bennett, S. N. Dmitriev, J. G. Ezold, J. H. Hamilton, R. A. Henderson, M. G. Itkis, Y. V. Lobanov, A. N. Mezentsev, K. J. Moody, S. L. Nelson, A. N. Polyakov, C. E. Porter, A. V. Ramayya, F. D. Riley, J. B. Roberto, M. A. Ryabinin *et al.*, Synthesis of a New Element With Atomic Number $Z = 117$, Phys. Rev. Lett. **104**, 142502 (2010).

[8] Y. T. Oganessian, V. K. Utyonkov, Y. V. Lobanov, F. S. Abdullin, A. N. Polyakov, R. N. Sagaidak, I. V. Shirokovsky, Y. S. Tsyganov, A. A. Voinov, A. N. Mezentsev, V. G. Subbotin, A. M. Sukhov, K. Subotic, V. I. Zagrebaev, S. N. Dmitriev, R. A. Henderson, K. J. Moody, J. M. Kenneally, J. H. Landrum, D. A. Shaughnessy *et al.*, Attempt to produce element 120 in the ^{244}Pu + ^{58}Fe reaction, Phys. Rev. C **79**, 024603 (2009).

[9] E. M. Kozulin, G. N. Knyazheva, I. M. Itkis, M. G. Itkis, A. A. Bogachev, L. Krupa, T. A. Loktev, S. V. Smirnov, V. I. Zagrebaev, J. Äystö, W. H. Trzaska, V. A. Rubchenya, E. Vardaci, A. M. Stefanini, M. Cinausero, L. Corradi, E. Fioretto, P. Mason, G. F. Prete, R. Silvestri *et al.*, Investigation of the reaction ^{64}Ni + ^{238}U being an option of synthesizing element 120, Phys. Lett. B **686**, 227 (2010).

[10] S. Hofmann, S. Heinz, R. Mann, J. Maurer, G. Münzenberg, S. Antalic, W. Barth, H. G. Burkhard, L. Dahl, K. Eberhardt, R. Grzywacz, J. H. Hamilton, R. A. Henderson, J. M. Kenneally, B. Kindler, I. Kojouharov, R. Lang, B. Lommel, K. Miernik, D. Miller *et al.*, Review of even element super-heavy nuclei and search for element 120, Eur. Phys. J. A **52**, 180 (2016).

[11] J. Khuyagbaatar, A. Yakushev, C. E. Düllmann, D. Ackermann, L.-L. Andersson, M. Asai, M. Block, R. A. Boll, H. Brand, D. M. Cox, M. Dasgupta, X. Derkx, A. Di Nitto, K. Eberhardt, J. Even, M. Evers, C. Fahlander, U. Forsberg, J. M. Gates, N. Gharibyan *et al.*, Search for elements 119 and 120, Phys. Rev. C **102**, 064602 (2020).

[12] H. M. Albers, J. Khuyagbaatar, D. J. Hinde, I. P. Carter, K. J. Cook, M. Dasgupta, Ch. E. Düllmann, K. Eberhardt, D. Y. Jeung, S. Kalkal, B. Kindler, N. R. Lobanov, B. Lommel, C. Mokry, E. Prasad, D. C. Rafferty, J. Runke, K. Sekizawa, C. Sengupta, C. Simenel *et al.*, Zeptosecond contact times for element $Z = 120$ synthesis, Phys. Lett. B **808**, 135626 (2020).

[13] K. Hagino and N. Takigawa, Subbarrier fusion reactions and many-particle quantum tunneling, Prog. Theor. Phys. **128**, 1061 (2012).

[14] B. B. Back, H. Esbensen, C. L. Jiang, and K. E. Rehm, Recent developments in heavy-ion fusion reactions, Rev. Mod. Phys. **86**, 317 (2014).

[15] W. J. Świątecki, K. Siwek-Wilczyńska, and J. Wilczyński, Fusion by diffusion. II. Synthesis of transfermium elements in cold fusion reactions, Phys. Rev. C **71**, 014602 (2005).

[16] V. I. Zagrebaev and W. Greiner, Cross sections for the production of superheavy nuclei, Nucl. Phys. A **944**, 257 (2015).

[17] B. Wang, K. Wen, W.-J. Zhao, E.-G. Zhao, and S.-G. Zhou, Systematics of capture and fusion dynamics in heavy-ion collisions, At. Data Nucl. Data Tables **114**, 281 (2017).

[18] H.-G. Clerc, J. G. Keller, C.-C. Sahm, K.-H. Schmidt, H. Schulte, and D. Vermeulen, Fusion-fission and neutron-evaporation-residue cross-sections in ^{40}Ar- and ^{50}Ti-induced fusion reactions, Nucl. Phys. A **419**, 571 (1984).

[19] A. J. Pacheco, J. O. Fernández Niello, D. E. DiGregorio, M. di Tada, J. E. Testoni, Y. Chan, E. Chávez, S. Gazes, E. Plagnol, and R. G. Stokstad, Capture reactions in the ^{40,48}Ca + ^{197}Au and ^{40,48}Ca + ^{208}Pb systems, Phys. Rev. C **45**, 2861 (1992).

[20] E. Prokhorova, A. Bogachev, M. Itkis, I. Itkis, G. Knyazheva, N. Kondratiev, E. Kozulin, L. Krupa, Y. Oganessian, I. Pokrovsky, V. Pashkevich, and A. Rusanov, The fusion–fission and quasi–fission processes in the reaction ^{48}Ca + ^{208}Pb at energies near the Coulomb barrier, Nucl. Phys. A **802**, 45 (2008).

[21] K. Banerjee, D. J. Hinde, M. Dasgupta, E. C. Simpson, D. Y. Jeung, C. Simenel, B. M. A. Swinton-Bland, E. Williams, I. P. Carter, K. J. Cook, H. M. David, C. E. Düllmann, J. Khuyagbaatar, B. Kindler, B. Lommel, E. Prasad, C. Sengupta, J. F. Smith, K. Vo-Phuoc, J. Walshe *et al.*, Mechanisms Suppressing Superheavy Element Yields in Cold Fusion Reactions, Phys. Rev. Lett. **122**, 232503 (2019).

[22] G. G. Adamian, N. V. Antonenko, S. P. Ivanova, and W. Scheid, Analysis of survival probability of superheavy nuclei, Phys. Rev. C **62**, 064303 (2000).

[23] N. V. Antonenko, E. A. Cherepanov, A. K. Nasirov, V. P. Permjakov, and V. V. Volkov, Competition between complete fusion and quasi-fission in reactions between massive nuclei. The fusion barrier, Phys. Lett. B **319**, 425 (1993).

[24] G. G. Adamian, N. V. Antonenko, W. Scheid, and V. V. Volkov, Treatment of competition between complete fusion and quasi-fission in collisions of heavy nuclei, Nucl. Phys. A **627**, 361 (1997).

[25] Z.-Q. Feng, G.-M. Jin, F. Fu, and J.-Q. Li, Production cross sections of superheavy nuclei based on dinuclear system model, Nucl. Phys. A **771**, 50 (2006).

[26] L. Zhu, W.-J. Xie, and F.-S. Zhang, Production cross sections of superheavy elements $Z = 119$ and 120 in hot fusion reactions, Phys. Rev. C **89**, 024615 (2014).

[27] N. Wang, E.-G. Zhao, W. Scheid, and S.-G. Zhou, Theoretical study of the synthesis of superheavy nuclei with $Z = 119$ and 120 in heavy-ion reactions with trans-uranium targets, Phys. Rev. C **85**, 041601(R) (2012).

[28] Z.-H. Liu and J.-D. Bao, Calculation of the evaporation residue cross sections for the synthesis of the superheavy element $Z = 119$ via the ^{50} Ti+^{249}Bk hot fusion reaction, Phys. Rev. C **84**, 031602(R) (2011).

[29] T. Cap, K. Siwek-Wilczyńska, and J. Wilczyński, Nucleus-nucleus cold fusion reactions analyzed with the l-dependent "fusion by diffusion" model, Phys. Rev. C **83**, 054602 (2011).

[30] T. Cap, K. Siwek-Wilczyńska, M. Kowal, and J. Wilczyński, Calculations of the cross sections for the synthesis of new $^{293-296}$118 isotopes in $^{249-252}$Cf(^{48} Ca, xn) reactions, Phys. Rev. C **88**, 037603 (2013).

[31] X. J. Bao, S. Q. Guo, H. F. Zhang, and J. Q. Li, Influence of entrance channel on production cross sections of superheavy nuclei, Phys. Rev. C **96**, 024610 (2017).

[32] K. Hagino, Hot fusion reactions with deformed nuclei for synthesis of superheavy nuclei: An extension of the fusion-by-diffusion model, Phys. Rev. C **98**, 014607 (2018).

[33] X.-J. Lv, Z.-Y. Yue, W.-J. Zhao, and B. Wang, Theoretical study of evaporation-residue cross sections of superheavy nuclei, Phys. Rev. C **103**, 064616 (2021).

[34] W. Loveland, Synthesis of transactinide nuclei using radioactive beams, Phys. Rev. C **76**, 014612 (2007).

[35] R. S. Naik, W. Loveland, P. H. Sprunger, A. M. Vinodkumar, D. Peterson, C. L. Jiang, S. Zhu, X. Tang, E. F. Moore, and P. Chowdhury, Measurement of the fusion probability $P_{\rm CN}$ for the reaction of ^{50}Ti with ^{208}Pb, Phys. Rev. C **76**, 054604 (2007).

[36] R. Yanez, W. Loveland, J. S. Barrett, L. Yao, B. B. Back, S. Zhu, and T. L. Khoo, Measurement of the fusion probability, $P_{\rm CN}$, for hot fusion reactions, Phys. Rev. C **88**, 014606 (2013).

[37] H. Lü, D. Boilley, Y. Abe, and C. Shen, Synthesis of superheavy elements: Uncertainty analysis to improve the predictive power of reaction models, Phys. Rev. C **94**, 034616 (2016).

[38] V. Zagrebaev and W. Greiner, Synthesis of superheavy nuclei: A search for new production reactions, Phys. Rev. C **78**, 034610 (2008).

[39] A. C. Berriman, D. J. Hinde, M. Dasgupta, C. R. Morton, R. D. Butt, and J. O. Newton, Unexpected inhibition of fusion in nucleus–nucleus collisions, Nature (London) **413**, 144 (2001).

[40] J. Khuyagbaatar, K. Nishio, S. Hofmann, D. Ackermann, M. Block, S. Heinz, F. P. Heßberger, K. Hirose, H. Ikezoe, B. Kinlder, B. Lommel, H. Makii, S. Mitsuoka, I. Nishinaka, T. Ohtsuki, Y. Wakabayashi, and S. Yan, Evidence for hindrance in fusion between sulfur and lead nuclei, Phys. Rev. C **86**, 064602 (2012).

[41] C. J. Lin, R. du Rietz, D. J. Hinde, M. Dasgupta, R. G. Thomas, M. L. Brown, M. Evers, L. R. Gasques, and M. D. Rodriguez, Systematic behavior of mass distributions in ^{48}Ti-induced fission at near-barrier energies, Phys. Rev. C **85**, 014611 (2012).

[42] K. Hammerton, Z. Kohley, D. J. Hinde, M. Dasgupta, A. Wakhle, E. Williams, V. E. Oberacker, A. S. Umar, I. P. Carter, K. J. Cook, J. Greene, D. Y. Jeung, D. H. Luong, S. D. McNeil, C. S. Palshetkar, D. C. Rafferty, C. Simenel, and K. Stiefel, Reduced quasifission competition in fusion reactions forming neutron-rich heavy elements, Phys. Rev. C **91**, 041602(R) (2015).

[43] B. B. Back, Complete fusion and quasifission in reactions between heavy ions, Phys. Rev. C **31**, 2104 (1985).

[44] M. Tsang, H. Utsunomiya, C. Gelbke, W. Lynch, B. Back, S. Saini, P. Baisden, and M. McMahan, Energy dependence of fission fragment angular distributions for ^{19}F, ^{24}Mg and ^{28}Si induced reactions on ^{208}Pb, Phys. Lett. B **129**, 18 (1983).

[45] K. Banerjee, D. Hinde, M. Dasgupta, J. Sadhukhan, E. Simpson, D. Jeung, C. Simenel, B. Swinton-Bland, E. Williams, L. Bezzina, I. Carter, K. Cook, H. Albers, C. Düllmann, J. Khuyagbaatar, B. Kindler, B. Lommel, C. Mokry, E. Prasad, J. Runke *et al.*, Sensitive search for near-symmetric and super-asymmetric fusion-fission of the superheavy element flerovium ($Z = 114$), Phys. Lett. B **820**, 136601 (2021).

[46] D. Hinde, M. Dasgupta, and E. Simpson, Experimental studies of the competition between fusion and quasifission in the formation of heavy and superheavy nuclei, Prog. Part. Nucl. Phys. **118**, 103856 (2021).

[47] A. S. Umar and V. E. Oberacker, Heavy-ion interaction potential deduced from density-constrained time-dependent Hartree-Fock calculation, Phys. Rev. C **74**, 021601(R) (2006).

[48] K. Wen, F. Sakata, Z.-X. Li, X.-Z. Wu, Y.-X. Zhang, and S.-G. Zhou, Non-Gaussian Fluctuations and Non-Markovian Effects in the Nuclear Fusion Process: Langevin Dynamics Emerging from Quantum Molecular Dynamics Simulations, Phys. Rev. Lett. **111**, 012501 (2013).

[49] C. Simenel, M. Dasgupta, D. J. Hinde, and E. Williams, Microscopic approach to coupled-channels effects on fusion, Phys. Rev. C **88**, 064604 (2013).

[50] K. Washiyama and D. Lacroix, Energy dependence of the nucleus-nucleus potential close to the Coulomb barrier, Phys. Rev. C **78**, 024610 (2008).

[51] C. Simenel, Nuclear quantum many-body dynamics, Eur. Phys. J. A **48**, 152 (2012).

[52] T. Nakatsukasa, K. Matsuyanagi, M. Matsuo, and K. Yabana, Time-dependent density-functional description of nuclear dynamics, Rev. Mod. Phys. **88**, 045004 (2016).

[53] C. Simenel and A. Umar, Heavy–ion collisions and fission dynamics with the time–dependent Hartree–Fock theory and its extensions, Prog. Part. Nucl. Phys. **103**, 19 (2018).

[54] P. Stevenson and M. Barton, Low-energy heavy-ion reactions and the Skyrme effective interaction, Prog. Part. Nucl. Phys. **104**, 142 (2019).

[55] K. Sekizawa, TDHF theory and its extensions for the multinucleon transfer reaction: A mini review, Front. Phys. **7**, 20 (2019).

[56] L. Guo, C. Shen, C. Yu, and Z. Wu, Isotopic trends of quasifission and fusion-fission in the reactions ^{48}Ca + ^{239,244}pu, Phys. Rev. C **98**, 064609 (2018).

[57] C. Simenel, R. Keser, A. S. Umar, and V. E. Oberacker, Microscopic study of ^{16}O + ^{16}O fusion, Phys. Rev. C **88**, 024617 (2013).

[58] L. Guo, C. Simenel, L. Shi, and C. Yu, The role of tensor force in heavy-ion fusion dynamics, Phys. Lett. B **782**, 401 (2018).

[59] K. Sekizawa and K. Hagino, Time–dependent Hartree–Fock plus Langevin approach for hot fusion reactions to synthesize the $Z = 120$ superheavy element, Phys. Rev. C **99**, 051602(R) (2019).

[60] L. Guo and T. Nakatsukasa, Time-dependent Hartree-Fock studies of the dynamical fusion threshold, EPJ Web Conf. **38**, 09003 (2012).

[61] A. S. Umar and V. E. Oberacker, ^{64}Ni+^{64}Ni fusion reaction calculated with the density-constrained time-dependent Hartree-Fock formalism, Phys. Rev. C **77**, 064605 2008.

[62] A. S. Umar, V. E. Oberacker, J. A. Maruhn, and P.-G. Reinhard, Entrance channel dynamics of hot and cold fusion reactions leading to superheavy elements, Phys. Rev. C **81**, 064607 (2010).

[63] A. S. Umar, C. Simenel, and V. E. Oberacker, Energy dependence of potential barriers and its effect on fusion cross-sections, Phys. Rev. C **89**, 034611 (2014).

[64] A. S. Umar, V. E. Oberacker, and C. Simenel, Fusion and quasifission dynamics in the reactions ^{48}Ca+^{249}Bk and ^{50}Ti+^{249}Bk using TDHF, Phys. Rev. C **94**, 024605 (2016).

[65] L. Guo, K. Godbey, and A. S. Umar, Influence of the tensor force on the microscopic heavy-ion interaction potential, Phys. Rev. C **98**, 064607 (2018).

[66] K. Godbey, L. Guo, and A. S. Umar, Influence of the tensor interaction on heavy-ion fusion cross sections, Phys. Rev. C **100**, 054612 (2019).

[67] C. Simenel, A. S. Umar, K. Godbey, M. Dasgupta, and D. J. Hinde, How the Pauli exclusion principle affects fusion of atomic nuclei, Phys. Rev. C **95**, 031601(R) (2017).

[68] N. Wang, X. Wu, Z. Li, M. Liu, and W. Scheid, Applications of Skyrme energy-density functional to fusion reactions for synthesis of superheavy nuclei, Phys. Rev. C **74**, 044604 (2006).

[69] K. Hagino, N. Rowley, and A. T. Kruppa, A program for coupled-channel calculations with all order couplings for heavy-ion fusion reactions, Comput. Phys. Commun. **123**, 143 (1999).

[70] C. Y. Wong, Interaction Barrier in Charged-Particle Nuclear Reactions, Phys. Rev. Lett. **31**, 766 (1973).

[71] V. E. Oberacker, A. S. Umar, and C. Simenel, Dissipative dynamics in quasifission, Phys. Rev. C **90**, 054605 (2014).

[72] A. Wakhle, C. Simenel, D. J. Hinde, M. Dasgupta, M. Evers, D. H. Luong, R. du Rietz, and E. Williams, Interplay between Quantum Shells and Orientation in Quasifission, Phys. Rev. Lett. **113**, 182502 (2014).

[73] A. S. Umar, V. E. Oberacker, and C. Simenel, Shape evolution and collective dynamics of quasifission in the time-dependent Hartree-Fock approach, Phys. Rev. C **92**, 024621 (2015).

[74] K. Sekizawa and K. Yabana, Time-dependent Hartree-Fock calculations for multinucleon transfer and quasifission processes in the ^{64}Ni + ^{238}U reaction, Phys. Rev. C **93**, 054616 (2016).

[75] W. J. Świątecki, K. Siwek-Wilczyńska, and J. Wilczyński, Fusion by diffusion, Acta Phys. Pol. B **34**, 2049 (2003).

[76] K. Siwek-Wilczyńska, T. Cap, M. Kowal, A. Sobiczewski, and J. Wilczyński, Predictions of the fusion-by-diffusion model for the synthesis cross sections of $Z = 114 - 120$ elements based on macroscopic-microscopic fission barriers, Phys. Rev. C **86**, 014611 (2012).

[77] J. Maruhn, P.-G. Reinhard, P. Stevenson, and A. Umar, The TDHF code Sky3D, Comput. Phys. Commun. **185**, 2195 (2014).

[78] G.-F. Dai, L. Guo, E.-G. Zhao, and S.-G. Zhou, Dissipation dynamics and spin-orbit force in time-dependent Hartree-Fock theory, Phys. Rev. C **90**, 044609 (2014).

[79] Z. Wu and L. Guo, Microscopic studies of production cross sections in multinucleon transfer reaction ^{58}Ni + ^{124}Sn, Phys. Rev. C **100**, 014612 (2019).

[80] X. Li, Z. Wu, and L. Guo, Entrance-channel dynamics in the reaction ^{40}Ca + ^{208}Pb, Sci. China: Phys., Mech. Astron. **62**, 122011 (2019).

[81] Z. Wu and L. Guo, Production of proton-rich actinide nuclei in the multinucleon transfer reaction ^{58}Ni + ^{232}Th, Sci. China: Phys., Mech. Astron. **63**, 242021 (2020).

[82] Z. Wu, L. Guo, Z. Liu, and G. Peng, Production of proton-rich nuclei in the vicinity of ^{100}Sn via multinucleon transfer reactions, Phys. Lett. B **825**, 136886 (2022).

[83] E. Chabanat, P. Bonche, P. Haensel, J. Meyer, and R. Schaeffer, A Skyrme parametrization from subnuclear to neutron star densities part II. Nuclei far from stabilities, Nucl. Phys. A **635**, 231 (1998).

[84] X.-X. Sun, L. Guo, and A. S. Umar, Microscopic study of the fusion reactions ^{40,48}Ca + ^{78}Ni and the effect of the tensor force, Phys. Rev. C **105**, 034601 (2022).

[85] K. Washiyama, Microscopic analysis of fusion hindrance in heavy nuclear systems, Phys. Rev. C **91**, 064607 (2015).

[86] R. Bock, Y. T. Chu, M. Dakowski, A. Gobbi, E. Grosse, A. Olmi, H. Sann, D. Schwalm, U. Lynen, W. Müller, S. Bjørnholm, H. Esbensen, W. Wölfli, and E. Morenzoni, Dynamics of the fusion process, Nucl. Phys. A **388**, 334 (1982).

[87] J. O. Newton, R. D. Butt, M. Dasgupta, D. J. Hinde, I. I. Gontchar, C. R. Morton, and K. Hagino, Systematics of precise nuclear fusion cross sections: The need for a new dynamical treatment of fusion? Phys. Lett. B **586**, 219 (2004).

[88] J. O. Newton, R. D. Butt, M. Dasgupta, D. J. Hinde, I. I. Gontchar, C. R. Morton, and K. Hagino, Systematic failure of the Woods-Saxon nuclear potential to describe both fusion and elastic scattering: Possible need for a new dynamical approach to fusion, Phys. Rev. C **70**, 024605 (2004).

[89] T. Cap, M. Kowal, and K. Siwek-Wilczyńska, Diffusion as a possible mechanism controlling the production of superheavy nuclei in cold fusion reactions, Phys. Rev. C **105**, L051601 (2022).

[90] T. Cap, K. Siwek-Wilczyńska, and J. Wilczyński, No chance for synthesis of super-heavy nuclei in fusion of symmetric systems, Phys. Lett. B **736**, 478 (2014).

[91] P. Jachimowicz, M. Kowal, and J. Skalski, Properties of heaviest nuclei with $98 \leqslant Z \leqslant 126$ and $134 \leqslant N \leqslant 192$, At. Data Nucl. Data Tables **138**, 101393 (2021).